Educational Administration: Theory and Practice
2024,30(1), 3136-3141
ISSN:2148-2403
https://kuey.net/

Research Article

Green Synthesis, Characterization, Structural, And Biological Properties Of Fe_2O_3 And Mno_2 Nanoparticles With Moringa Oleifera Fruit Extract

Shital Shivaji Bankar[1], Anita Kashinath Kshirsagar[1], Priyanka Ganesh Bhutekar[1], Ratnamala Tanaji More[1], Suresh Tanhaji More[2], Shivaji Baburao Munde[3*]

[1]P.G. Department of Chemistry, Jalna Education Society's, R. G. Bagdia Arts, S. B. Lakhotia Commerce, and R. Bezonji Science College, Jalna-431203 (M.S.).
[2]Dept of Chemistry, VPMK'S Art's Commerce and Science College Kinhavali, Maharashtra 421403.
[3*]Department of Chemistry, Shri Muktanand College Gangapur, Aurangabad -431001 (M.S.)

***Corresponding author:** Shivaji Baburao Munde
*(e-mail: principalsbmunde@gmail.com)

Citation: Shivaji Baburao Munde, et.al (2024), Green Synthesis, Characterization, Structural, And Biological Properties Of Fe_2O_3 And Mno_2 Nanoparticles With Moringa Oleifera Fruit Extract, *Educational Administration: Theory and Practice*, *30*(1), 3136-3141
Doi: 10.53555/kuey.v30i1.7057

ARTICLE INFO

ABSTRACT

Researchers are closely studying Fe_2O_3 and MnO_2 nanoparticles (NPs) for their various applications in areas such as photocatalytic degradation activity, medicine, and optics. We utilized an environmentally friendly approach to produce Fe_2O_3 and MnO_2 NPs for the present study. Moringa Oleifera fruit extract functioned as a gelling and reducing agent, while ferric and manganese chlorides were used as precursors to produce nanoparticles. The structural and morphological properties of the NPs were analyzed using SEM, FT-IR, XRD, EDX, and UV-visible spectroscopy. The nanoparticles exhibited potent antibacterial and antifungal properties against both gram-negative and gram-positive bacteria, as well as fungal species. They have also evaluated significant antibacterial activity against the same bacteria and types of fungal species. The study concluded that Fe_2O_3 and MnO_2 NPs had promising antibacterial properties.

Key words: Nanomaterials; FT-IR; SEM; Antibacterial activity; Fe_2O_3 and MnO_2 nanoparticles

INTRODUCTION

Nanostructured metal oxides exhibit unique properties such as optical, photocatalytic degradation activity, semiconducting, and insulating behaviour, distinguishing them from their larger forms [1]. Researchers are intrigued by ferrous oxide nanoparticles due to their potent photocatalytic activity, cost-effectiveness, simple manufacturing process, and unique optical, magnetic, and electrical properties, among other factors [2]. They exhibit a high excitation binding energy of 60 meV at ambient temperature, a band gap energy of 3.35 eV, and demonstrate good UV absorbance and antibacterial properties. Various techniques have been used to create ferric oxide nanoparticles, including hydrothermal, sol-gel, chemical precipitation, and microwave irradiation. These nanoparticles can be altered by doping them with metallic ions [3]. They can serve as foundational elements for magnetic semiconductors, photocatalysts, gas sensors, light-emitting components, solar cells, field-effect transistors, and biological systems. Ferrous chloride, potassium permanganate, and moringa oleifera fruit extract were used in creating Fe_2O_3 and MnO_2 NPs. This technology offers good quality, low processing temperature, cost-effective processing, and a greater yield compared to other methods.

EXPERIMENTAL

Green Synthesis of Nanoparticles

The gathered fruit of the chosen weed plant was cleaned to eliminate dust particles and then dried in the shade at room temperature for a specific timeframe. Dried fruit was crushed and ground into a fine powder. The powdered fruit of moringa oleifera was used to prepare an extract using a Soxhlet extractor and triple distilled water as the solvent. The colloidal solution extracted is centrifuged and filtered through Whatman paper to eliminate plant residues, then kept in a refrigerator at 4°C for future use.

Ferric oxide nanoparticles (Fe_2O_3-NPs) were prepared using an environmentally friendly method. A 0.01M solution of [$Fe(Cl)_3$] was produced in triply distilled water. The moringa oleifera fruit extract was gradually added in a specific ratio while continuously swirling with a magnetic stirrer until a brown colloidal solution was formed. The colloidal solution was centrifuged at 10,000 rpm for a specific period. The centrifuged particles were rinsed 2-3 times with distilled water. The centrifuged particles were separated and then dried in a hot air oven at 60°C. The Fe_2O_3-NPs were kept in a plastic tube vial at room temperature.

MnO_2-NPs were prepared in an eco-friendly manner. In triply distilled water, a 0.01M solution of [$KMnO_4$] was obtained. Until a brown colloidal solution formed, the moringa oleifera fruit extract was added gradually in a predetermined ratio while being constantly swirled with a magnetic stirrer. For a predetermined amount of time, the colloidal solution was centrifuged at 10,000 rpm. Two or three times, distilled water was used to rinse the centrifuged particles. After being separated, the centrifuged particles were dried at 60°C in a hot air oven. The MnO_2-NPs were stored at room temperature in a plastic tube vial.

Characterization Methods

The research utilized CuK (= 1.5418) to generate an X-ray powder diffraction (XRD) pattern, analyzing its shape and elemental composition with a resolution scanning electron microscope. FT-IR spectra were obtained in the solid phase with the KBr pellet method, optical absorption spectra were obtained using a UV-Vis absorption spectrometer, and photoluminescence spectrum studies were conducted with a JY Fluorolog 3-11 spectrometer.

Antimicrobial Assay

Disc Preparation

6mm discs composed of Whatman No. 1 filter paper were sterilized at 121°C and subsequently dehydrated at 50°C in a hot air oven. Discs were created using solvent extraction and control methods.

Collection of test microorganisms

Konkan Gyanpeeth Rahul Dharkar College of Pharmacy and Research Institute, Karjat-India supplied gram-positive and gram-negative bacterial strains of *E. coli* and *B. subtilis* and collected strains of *C. albicans* and *S. cerevisiae* fungi.

Assay of Antibacterial Activity

The antibacterial activity was evaluated using the disc diffusion technique. The strain was cultivated in Mueller-Hinton broth for 12 hours at 37°C. Inoculated Mueller Hinton agar plates with a new inoculum containing 1 to 2, 106 CFU/ml. Plates with chemicals impregnated and solvent controls were incubated aerobically at 37°C. Negative solvent control discs were placed on top of each pathogen-inoculated plate. An aseptic environment was maintained consistently during the trial. The zone of inhibition (mm) for each metal was measured after 24 hours.

Assay of Antifungal Activity

The Bauer *et al.* (1966) approach was adapted for performing an antifungal activity test. The polydopamine antibacterial materials were prepared, sterilized using an autoclave, and then cooled to 45°C. Tartaric acid was added to the cooled liquid and then transferred onto sterilized petri dishes. The plates were inoculated with an appropriate microbiological solution and discs containing standard *fluconazole*, extracts from various solvents, and control samples were introduced. The areas around the paper disc were measured following a 72-hour incubation period at 28°C.

RESULTS AND DISCUSSION

Standard equipment and procedures were used to examine and analyze the Fe_2O_3 and MnO_2 nanoparticle synthesis results in an environmentally responsible way.

The formation of metal oxide nanoparticles was first detected by a change in the colour of the reaction mixture. Analyzing data from UV-vis and FTIR spectra led to the preparation of metal oxide nanoparticles.

XRD Spectral Analysis

Figure 1 displays the X-ray powder diffraction peaks of Fe_2O_3 and MnO_2 nanoparticles. Our green-prepared nanoparticles had an average diameter of around 20-40 nm and a spherical shape, according to the data obtained using scanning electron microscopy analysis (**Figure 1**).

The structure was characterized by XRD analysis. The existence of nanoparticles (Fe_2O_3 NPs), indicated by two peaks at 33.0902θ and 35.5602θ, was found in the sample.

Figure 1 shows that the presence of hematite structure is indicated by both of these peaks.

Figure 1 shows the XRD pattern of MnO_2 NPs when they were synthesized. Diffraction peaks at 2θ = 19.3°,

27.6°, 32.9°, 47.3°, 50.6°, and 60.9° were observed in the crystalline phases of MnO_2 NPs, which correspond to the (110), (200), (310), (500), and (451) crystal planes, respectively.

The cubic structure of the material with a lattice parameter of 4.45 Å is further shown by this. The fact that the indexed crystalline planes agreed well with the conventional values provided more evidence that MnO_2 is crystalline.

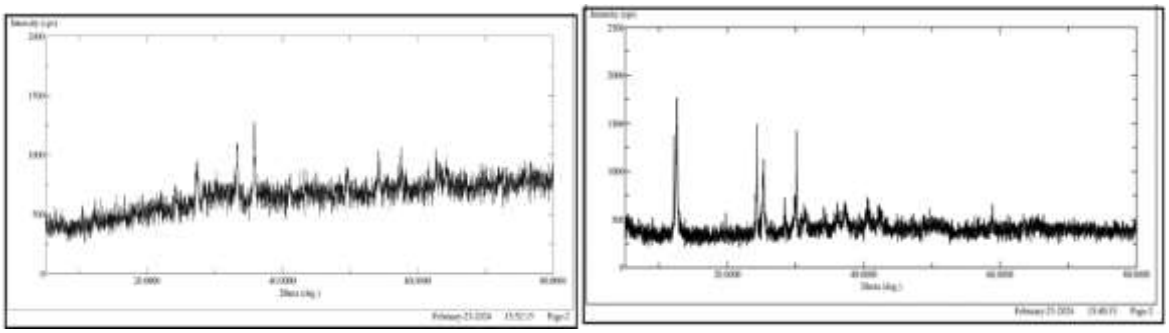

Figure 1. XRD spectra of *moringa oleifera* mediated Fe_2O_3 and MnO_2 NPs

FT-IR Spectral Analysis

The use of Fourier achieves functional group identification of active components transform infrared spectroscopy. Alcohol and phenolic compound O-H stretching were determined to be the source of the green-produced NPs' high absorption peak at 3180-3286 cm^{-1} for FTIR.

Ketones, aldehydes, and carboxylic acids all have stretching vibrations of CO groups, which caused the signal at 1622-1628 cm^{-1}. Absorption bands at 614-615 cm^{-1}, which correlate to the Fe-O and Mn-O bands (**Figure 2**), describe the preparation of Fe_2O_3 and MnO_2 NPs.

Figure 2 shows that the presence of Fe_2O_3 and MnO_2 nanoparticles in the sample was indicated by the absence of this peak in the corresponding plant extract.

Moringa oleifera fruit extract was found to be responsible for the bio-reduction of ferric chloride into iron oxide nanoparticles, as well as potassium permanganate to manganese dioxide, as validated by FTIR analysis [8,9].

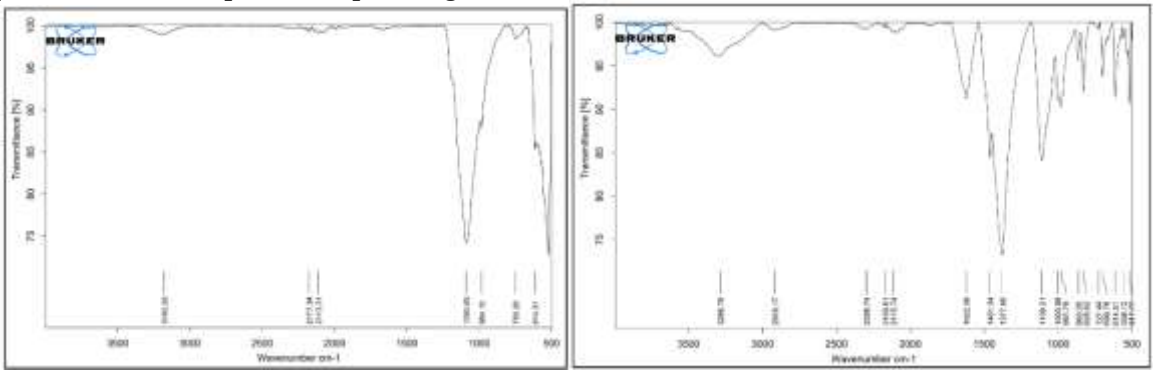

Figure 2: FTIR spectra of *moringa oleifera* mediated Fe_2O_3 and MnO_2 NPs

UV-Visible Spectral analysis

Figure 3 displays the UV-visible absorption spectra of pure Fe_2O_3 and MnO_2 nanoparticle samples. The absorption edges occur at wavelengths of 273-290 nm, 336-345 nm, and 370-398 nm. The absorption edges below 400 nm are due to charge transfer from the O; 2*p* and Fe and Mn; 3*d* states.

The absorption spectra of Fe_2O_3 and MnO_2 NPs show a red shift towards higher wavelengths, indicating the transition metal's integration into Fe_2O_3 and MnO_2-NPs lattice sites.

$\alpha h\upsilon = A(h\upsilon - E_g)^n$

The optical band gaps of pure Fe_2O_3 and MnO_2 NPs were determined to be 3.88eV, 3.77eV, and 3.42eV, respectively. Fe_2O_3 and MnO_2 NPs exhibited decreased band gap energy compared to pure Fe_2O_3 and MnO_2.

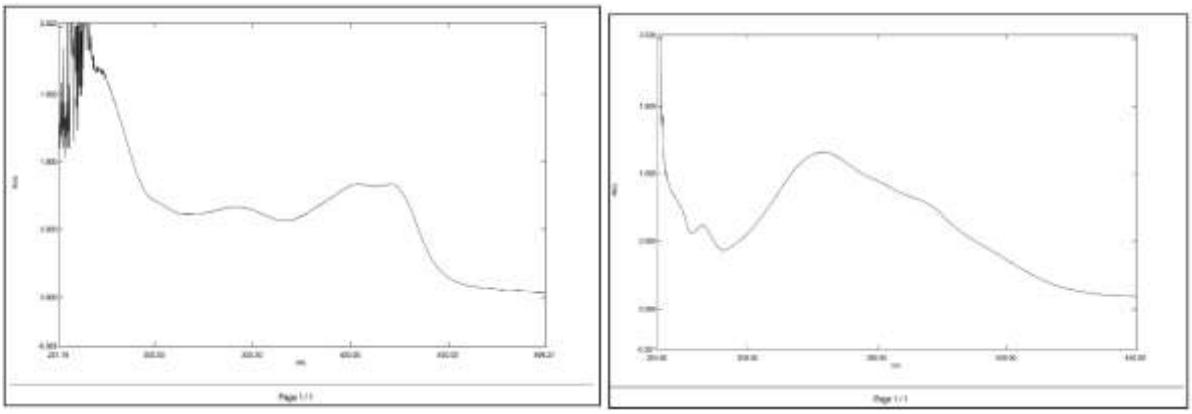

Figure 3: UV-vis spectra of *moringa oleifera* mediated Fe_2O_3 and MnO_2 NPs

SEM analysis

Figures 4 to **5** show the surface structure of pure Fe_2O_3 and MnO_2, and Fe_2O_3 and MnO_2 nanoparticles. The nanoparticles are usually within the nanometer scale and have spherical shapes.

Fe_2O_3 and MnO_2 nanoparticles feature small pores that expand in size because of the incorporation of Fe and Mn ions into Fe_2O_3 and MnO_2 lattice sites respectively. Transition metal was found to be potentially present.

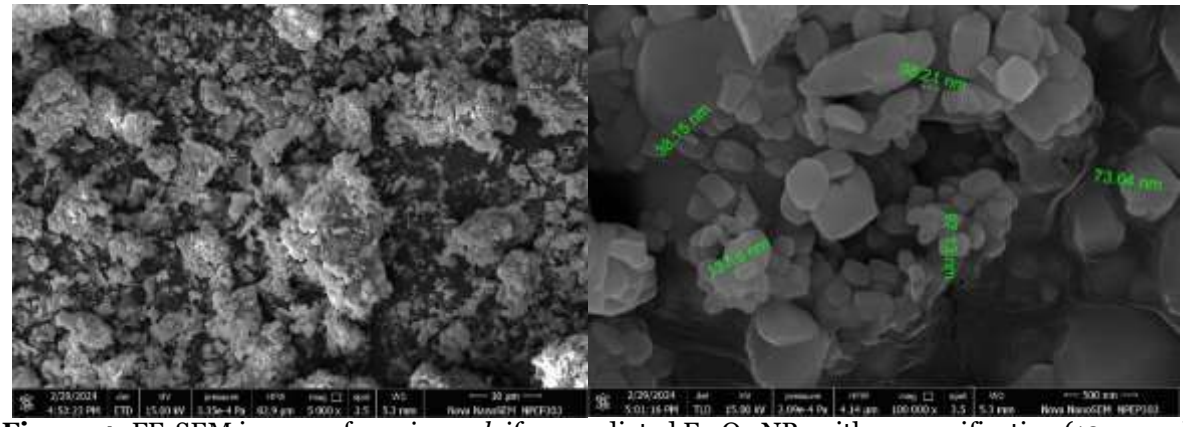

Figure 4: FE-SEM images of *moringa oleifera* mediated Fe_2O_3-NPs with a magnification (10µm and 500nm).

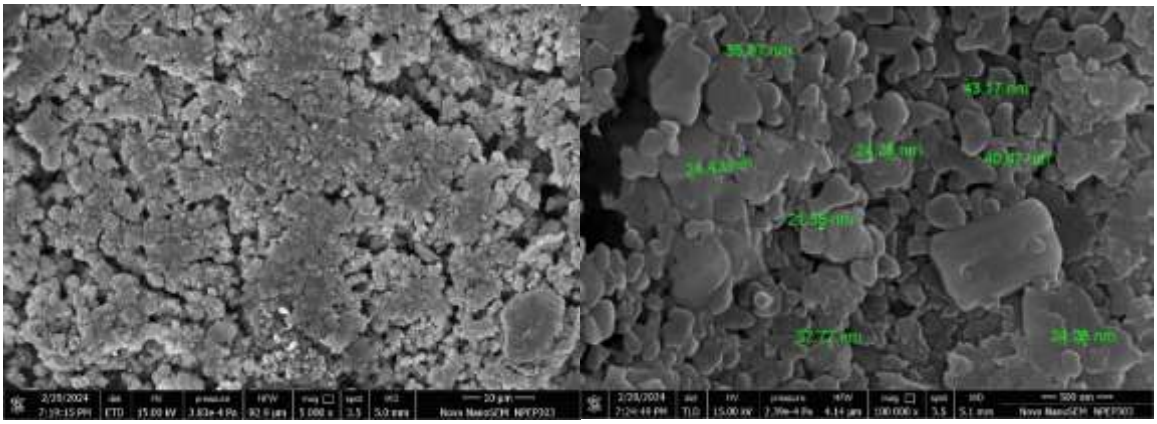

Figure 5: FE-SEM images of *moringa oleifera* mediated MnO_2-NPs with a magnification (10µm and 500nm).

EDAX analysis

The study examines the elemental composition of Fe_2O_3 and MnO_2 nanoparticles. The results indicate Fe^{3+} and Mn^{2+} ion concentrations of 2.30% and 6.25%, respectively. Manganese dioxide nanoparticles consist of 40% manganese and 60% oxygen by atomic proportion.

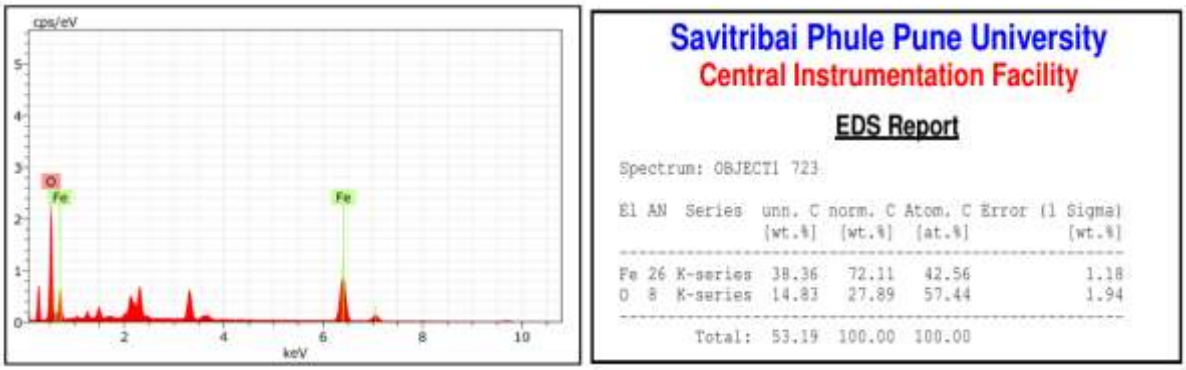

Figure 6: EDAX spectrum for *moringa oleifera* mediated Fe_2O_3-NPs

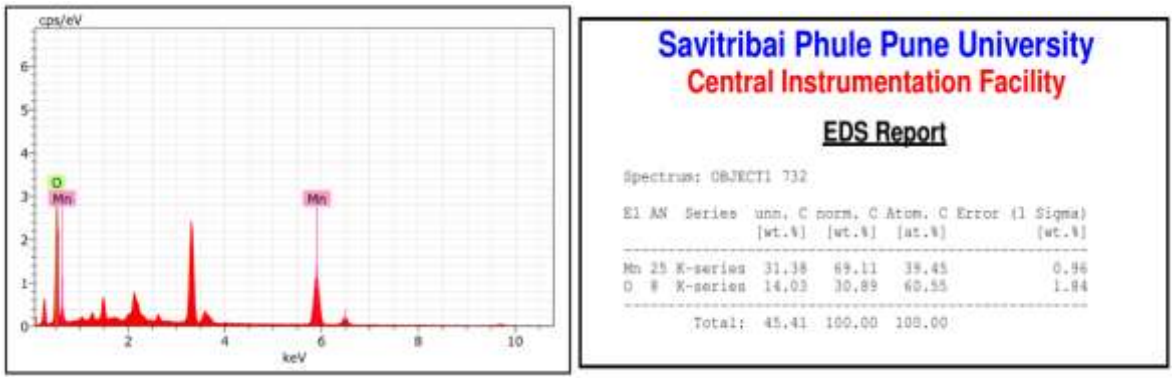

Figure 7: EDAX spectrum for *moringa oleifera* mediated MnO_2-NPs

Antibacterial activities

The study evaluated *Amphotericin-B* and *Ciprofloxacin*, two prominent antibacterial medications, and found that both molecules had potent antibacterial activity. The study aims to evaluate the antibiotic susceptibility pattern of Nuro pathogens to identify the causative agents of urinary tract infections (UTIs). Gram-positive B exhibited high antibacterial activity, with *S. subtilis* and *E. coli* being prevalent bacteria associated with UTIs. An antifungal drug was applied to *C. albicans*, and only NPs Fe_2O_3, and MnO_2 exhibited antifungal activity against *C. albicans*, but *S. cerevisiae* was not affected by any of the NPs.[21]

CONCLUSION

The study demonstrates the face-centred cubic structure of Fe_2O_3 and MnO_2 nanoparticles, which exhibit a spherical morphology as evidenced by XRD and SEM pictures. EDAX analysis verifies the elements' composition purity. Fe_2O_3 and MnO_2 nanoparticles are efficient in eliminating gram-positive bacteria C. albicans, S. cerevisiae, E. coli, and S. subtilis. The catalytic activity was evaluated in the presence of solar radiation using the chosen dye, which decreased in size with time.

REFERENCES

1. Ramola, B., Chandra, J., Ramola, M., Chhabra, J., and Singh, A. (2019) Green Synthesis, Characterisations and Antimicrobial Activities of CaO Nanoparticles. *Orie. J. Chem.*, 35(3),1154-1157. http://dx.doi.org/10.13005/ojc/350333.
2. Rong-Rong, L. (2019) Polyionic Liquids (PIL) Promoted Ce Doped ZnO for the Photocatalytic Degradation of Rhodamine B (RhB). *Eur. J. Chemical Soc.*, 4(36), 10748-10755. https://doi.org/10.1002/slct.201902040.
3. Siyu, L., Yuqin, M., and Lang, Z. (2022) Production of ZnO-CoOx-CeO_2 nanocomposites and their dye removal performance from wastewater by adsorption-photocatalysis, *J. Mole. Liqs*, 364, 119924. https://doi.org/10.1016/j.molliq.2022.119924.
4. Reddy Yadav, S.L. (2016) Fruit juice extract mediated synthesis of CeO_2 nanoparticles for antibacterial and photocatalytic activities. *Eur. Phys. J. Plus*, 5, 131-135. https://doi:10.1140/epjp/i2016-16154-y
5. Bauer. W.A, Kirby. M.W, Sherris C.J, and Turck.M, Antibiotic Susceptibility Testing by a Standardized Single Disk Method, Am J Clinical Path., 1996; 45:493-496. https://doi.org/10.1093/ajcp/45.4_ts.493.
6. Abbo, M., Hooton, M. (2014) Antimicrobial Stewardship and Urinary Tract Infections. *Antibiotics (Basel)*, 2, 174-92. https://doi.org/10.1016/j.jcrysgro.2008.01.011.
7. Chen, T. (2008) The effect of La doping concentration on the properties of zinc oxide films prepared by the sol-gel method. *J. Cryst. Growth*, 310, 2627–2632. https://doi.org/10.1016/j.jcrysgro.2008.01.011

8. Aisah, N., Gustiono, D., Fauzia, V., Sugihartono, I., Nuryadi, R. (2017) Synthesis and Enhanced photocatalytic activity of Ce-Doped ZnO_2 Nanorods by hydrothermal method. *Mater. Sci. Eng*, 172, 1-8. http://sipeg.unj.ac.id/repository/upload/artikel.
9. Siim, K., Protima, R., Erwan, R. (2018) Plant extract mediated synthesis of nanoparticles. *Emer., Appls. of Nps. and Archit. Nanosts.*, 411-446. https://doi.org/10.1016/B978-0-323-51254-1.00014-2.
10. Yoki, Y., Sudirman, D., Oky, B., Apriandanu, A., and Prasetiyo, W. (2019) Plant extract mediated synthesis of Au/TiO_2 nanocomposite and its photocatalytic activity under sodium light irradiation. *Comp. Coms.*, 16, 50-56. https://doi.org/10.1016/j.coco.2019.08.006.
11. Yoki, Y., Eny, K., Dewangga, O., Bagus, A., Nadya, N., and Datura, M. (2020) Leaves extract mediated CeO_2 nanoparticles: Synthesis, characterizations, and degradation activity of DPPH radical. *Surfaces and Interfaces*, 19, 100437. https://doi.org/10.1016/j.surfin.2020.100437.
12. Kontham, S. (2022) Review on the facile synthesis of cerium oxide nanoparticles and their biomedical applications. *Inorg. and Nano-Metal Chem.*, 52(8), 1183-1195. https://doi.org/10.1080/24701556.2021.1963284.
13. Wang, N. (2016) Hydrothermally synthesized CeO_2 nanowires for H_2S sensing at room temperature. *J. of Alloys and Comps.*, 682, 647-653. http://dx.doi.org/10.1016/j.jallcom.2016.04.311.
14. Elahi, B. (2018) Preparation of cerium oxide nanoparticles in Salvia Macrosiphon Boiss seeds extract and investigation of their photocatalytic activities. *Ceramics Inter.*, 45(4), 4790-4797. https://doi.org/10.1016/j.ceramint.2018.11.173.
15. Yadav, S. L. (2016) Fruit juice extract mediated synthesis of CeO2 nanoparticles for antibacterial and photocatalytic activities. *Eur. Phys. J. Plus*, 131(5). https://doi.org/10.1140/epjp/i2016-16154-y.
16. Manikandan, A., Durka, M., Selvi, A. M., and Arul Antony, S. (2016) Aloe vera Plant Extracted Green Synthesis, Structural and Opto-Magnetic Characterizations of Spinel $CoxZn\text{-}xAl_2O_4$ Nano-Catalysts. *J. Nanosci. Nanotechnol*, 16, 357-373. https://doi.org/10.1166/jnn.2016.10621.
17. Manikandan, A., Sridhar, R., Arul, S., and Ramakrishna, S., (2014) A simple aloe vera plant extracted microwave and conventional combustion synthesis: Morphological, optical, magnetic and catalytic properties of $CoFe_2O_4$ nanostructures. *J. Mol. Struct.*, 1076, 188- 200. http://dx.doi.org/10.1016/j.molstruc.2014.07.054.
18. Mathubala, G., Manikandan, A., Arul Antony, S., and Ramar, P. (2016) Enhanced Photocatalytic Activity of Spinel $CuxMn1\text{-}x\ Fe_2O_4$ Nanocatalysts for the Degradation of Methylene Blue Dye and Opto-Magnetic Properties. *Nanosci. Nanotech. Lett.*, 8, 375-381. https://doi.org/10.1166/nnl.2016.2149.
19. Mathubala, G., Manikandan, A., Arul Antony, S., and Ramar, P. (2016) Photocatalytic Degradation of Methylene Blue Dye and Magneto-Optical Studies of Magnetically Recyclable Spinel $NixMn1\text{-}xFe_2O_4$ (x = 0.0 - 1.0) Nanoparticles. *J. Mol. Struct.*, 1113, 79-87. https://doi.org/10.1016/j.molstruc.2016.02.032.
20. Anandan, S. (2007) Photocatalytic Activity of La-Diped ZnO for the Degradation of Monocrotophos in Aqueous Suspension. *J. Mol. Catal. A: Chem.*, 266, 149–157. http://dx.doi.org/10.1016/j.molcata.2006.11.008.
21. Godlyn Abraham, A. (2017) Enhanced Opto-Magneto Properties of Nix $Mg1\text{–}xFe_2O_4$ ($0.0 \leq x \leq 1.0$) Ferrites Nano-Catalysts. *J. Nanoelect. Optoelect.*, 12, 1326–1333. https://doi.org/10.1166/jno.2017.2299.
22. Wang, L., Hu, C. and Shoa, L. (2017) The antimicrobial activity of nanoparticles: present situation and prospects for the future. *International Journal of Nanomedicine*, 12, 1227–1249.